Anton Paar

MEASURING INSTRUMENTS FOR YOUR HARD COATINGS

- Find the solution you need in our industrial portfolio, the broadest on the market
- Set up and operate our robust instruments wherever you need them, in the lab or directly at your production site
- Use reference sample kits to verify instrument performance on your own schedule, giving you results you can rely on
- Get started quicker with an application-specific support database that helps you navigate challenges

Get in touch: **www.anton-paar.com**

ADVANCED MATERIALS INTERFACES
www.advmatinterfaces.de

Voltage Manipulation of Synthetic Antiferromagnetism in CoFeB/Ta/CoFeB Heterostructure for Spintronic Application

Wanjun Peng, Lei Wang, Yaojin Li, Yujing Du, Zhexi He, Chenying Wang, Yifan Zhao,* Zhuangde Jiang, Ziyao Zhou, and Ming Liu*

The synthetic antiferromagnets (SAFs) with inserted heavy metal tantalum (Ta) are attracting an increasing interest due to the relatively large spin Hall angles, resulting in a much lower driven current for low-power consumption, and the conduciveness to high magnetoresistance, showing more suitability for an application. Here, stable and reversible switching behavior is experimentally realized between antiferromagnetic (AFM) coupling and ferromagnetic (FM) coupling in $Co_{40}Fe_{40}B_{20}$/Ta/$Co_{40}Fe_{40}B_{20}$/(011) $Pb(Mg_{1/3}Nb_{2/3})O_3$-$PbTiO_3$ (PMN-PT) multiferroic heterostructures after applying an external voltage, proved by vibrating sample magnetometer (VSM) and ferromagnetic resonance (FMR) measurements. The indirect interaction shows no periodical oscillation with the layer thicknesses variation of FM layer or nonmagnetic (NM) layer experimentally, which is consistent with the previous reports in theoretical calculation. This work is instructive and guiding for a better understanding of SAFs and realizing the next generation of AFM spintronic devices.

1. Introduction

The synthetic antiferromagnets (SAFs), which is composed of two ferromagnetic (FM) layers separated by a nonmagnetic (NM) spacer, show great potential for developing novel spintronic applications such as artificial neural networks and high-density information storage.[1–11] The heavy metal tantalum (Ta) has been the most widely used in spintronics owing to the relatively large spin Hall angles.[12] The strong spin–orbit torques (SOTs) can be generated due to the spin Hall effect and the Rashba effect at the heavy metal/FM metal interface, which produce both a Slonczewski-like torque and a field-like torque.[13–17] These torques can be exerted on the adjacent FM layers to achieve magnetization switching. Besides, inserting a thin Ta layer can reduce boron composition in CoFeB due to its absorption of boron from the CoFeB layers, which benefits obtaining high magnetoresistance, showing great potential in the realization of next-generation spintronic devices.[18] Furthermore, it has been demonstrated in theory that interlayer exchange coupling (IEC) via Ta shows no oscillation as the thickness of the spacer changes,[19] and the indirect interaction is dependent on the FM layer's thickness.[20–22] However, few relevant works are reported experimentally to understand better the IEC within inserted Ta, which is crucial for the antiferromagnetic spintronics possessing ultrafast response and wide compatibility.

The tunability of SAFs is the leading edge in emerging spintronics.[8] The Ruderman–Kittel–Kasuya–Yosida (RKKY) interaction rooted in spin-dependent Friedel-like spatial oscillations can arise within SAF multilayers,[8] where the top and bottom FM layers can be indirectly coupled via the itinerant electrons in the NM middle layer.[23,24] The magnetic moments in two FM layers can be parallel or antiparallel arrangements, and IEC displays the periodical oscillations originated from FM layers' thicknesses.[25] To date, lots of progress has been achieved in regulating the magnetic properties of SAFs in situ by an electric field (*E*-field), considered an attractive research direction bringing the tunability to the next level,[8] as demonstrated experimentally recently.[7,26,27] For example, a voltage-controlled switch between FM and antiferromagnetic (AFM) coupling in CoFeB/Ru/CoFeB heterostructures via ionic liquid/gel; however, the interfacial chemical corrosion is inevitable.[7,27] Moreover, we tuned CoFeB/Ru/CoFeB/$Pb(Mg_{1/3}Nb_{2/3})O_3$-$PbTiO_3$ (PMN-PT) heterostructures via voltage-induced strain/stress change.[26] Nevertheless, the CoFeB/Ru/CoFeB structure is

W. Peng, Y. Li, Y. Du, Z. He, Y. Zhao, Z. Jiang, Z. Zhou, M. Liu
Electronic Materials Research Laboratory
Key Laboratory of the Ministry of Education & International Center for Dielectric Research
School of Electronic Science and Engineering
State Key Laboratory for Manufacturing Systems Engineering
Collaborative Innovation Center of High-End Manufacturing Equipment
Xi'an Jiaotong University
Xi'an 710049, China
E-mail: zhaoyifan100@xjtu.edu.cn

L. Wang
Center for Spintronics and Quantum Systems
State Key Laboratory for Mechanical Behavior of Materials
Xi'an Jiaotong University
Xi'an 710049, China
E-mail: wanglei.icer@xjtu.edu.cn

C. Wang, Y. Zhao, Z. Jiang, Z. Zhou, M. Liu
The International Joint Laboratory for Micro/Nano Manufacturing and Measurement Technology
Xi'an Jiaotong University
Xi'an 710049, China

The ORCID identification number(s) for the author(s) of this article can be found under https://doi.org/10.1002/admi.202200007.

DOI: 10.1002/admi.202200007

not technologically suitable for application owing to the relatively small spin Hall angle of Ru, which essentially limits its practical application. Continuous research of SAFs with Ta inserted is necessary for sufficient knowledge and satisfying major requirements for scientific and industrial needs thereby.

Here, we examined a tunable IEC in $Co_{40}Fe_{40}B_{20}$ (CFB)/Ta/CFB/(011) PMN-PT multiferroic heterostructures. The IEC was engineered by modulating the layer thickness of Ta or CFB respectively and by *E*-field through magnetoelectric coupling effect at room temperature. A series of SAF heterostructures were fabricated by DC magnetron sputtering. And results of the vibrating sample magnetometer (VSM) exhibited clear FM layer thickness (t_{CFB}) and NM layer thickness (t_{Ta}) dependences of the indirect interaction. The easy-axis magnetic hysteresis (*M*–*H*) loops switched between single S-shape and double S-shape, corresponding to FM coupling mode and AFM coupling mode, as the FM or NM layer thickness changed. And exchange coupling via Ta experimentally showed no periodical oscillation, indicating that the multilayers had a decent IEC effect for industrial manufacture because of the high robustness to layer thickness. Then, VSM and the ferromagnetic resonance (FMR) measurements systematically showed that a reversible and stable AFM-FM coupling transformation was realized after applying external *E*-field on (011) PMN-PT, which is more suitable for application than CoFeB/Ru/CoFeB[7,26,27] because of its great practical value in emerging SOT devices attributed to the large spin Hall angles of Ta. This transition phenomenon was related to the disturbance of the Fermi level and itinerant electrons,[7,27] which was originated from the *E*-field-induced lattice strain.[26,28,29]

2. Results and Discussions

By carefully engineering the IEC through depositing SAF multilayers with different t_{CFB} and t_{Ta}, the switching of AFM and FM modes is realized. **Figure 1**a illustrates the schematic of the trilayer. We deposit the thin amorphous Ta at the bottom as a buffer layer to improve the surface morphology of PMN-PT piezoelectric substrate and the Ta at the top as a capping layer to avoid oxidation.[30] Besides, the [100] direction is parallel to the easy axis because of the shape anisotropy resulting from the size ($5 \times 4 \times 0.5$ mm) of the PMN-PT single crystals. Figure 1b presents contour plots of the easy-axis loop recorded by sweeping static *H*-field (from – 40 to + 40 Oe along the [100] direction) when the FM layer thickness is 1.8 nm to investigate the effect of varying Ta spacer thicknesses. In this case, when t_{Ta} changes from 0.3 to 0.7 nm, the IEC between two FM layers gradually generates AFM coupling, demonstrated by a double S-shape. When t_{Ta} increases to 0.75 nm, the hysteresis loop transforms to a single-loop, indicating an FM coupling. It is generally accepted that the oscillatory indirect magnetic exchange coupling via the inset layer, caused by the hybridization between the 3d bands of the FM layers and the conduction band of the NM layer, is a general phenomenon.[8] However, this SAF structure always shows an FM coupling behavior when the inserted Ta becomes thicker (>0.75 nm) or thinner (<0.65 nm), which is consistent with the previous theoretical studies.[19] Figure 1c,d, and Figure S1 (Supporting Information) show the magnetic hysteresis loops for SAF heterostructures, where t_{Ta} ranges from 0.3 to 1.2 nm. The experiments

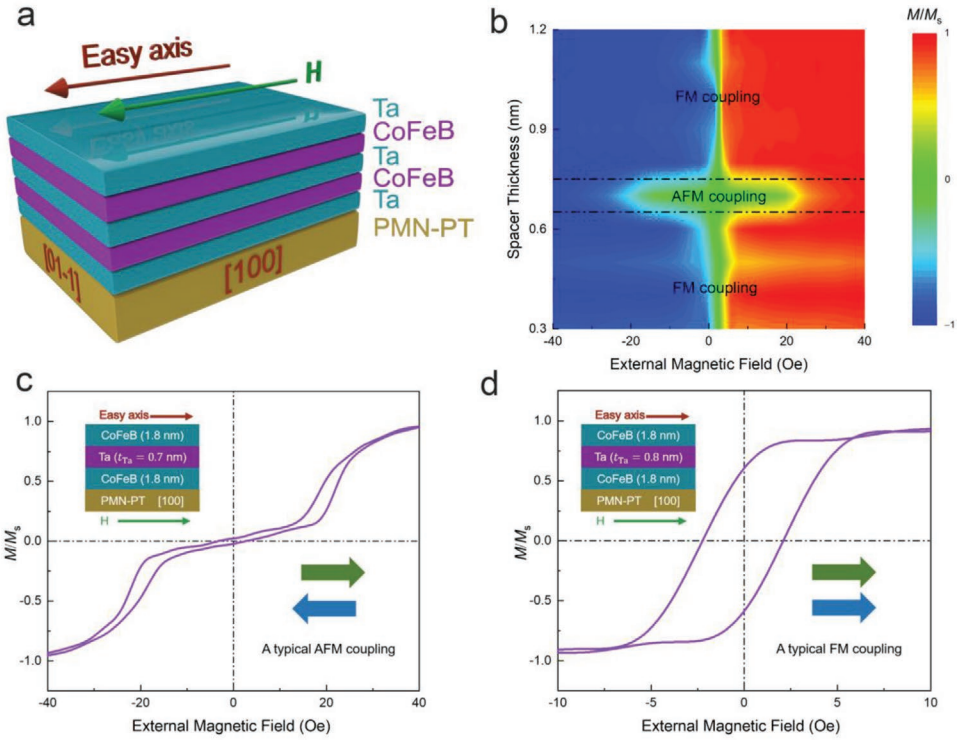

Figure 1. a) Structure of the tunable SAF multiferroic heterostructure. b) Contour plots of the easy-axis loop recorded by the sweeping static magnetic field (increasing from – 40 to + 40 Oe along the [100] direction of PMN-PT), which indicate NM interlayer thickness dependence of IEC. c,d) Magnetic hysteresis loops at c) t_{Ta} = 0.7 nm and d) t_{Ta} = 0.8 nm, respectively.

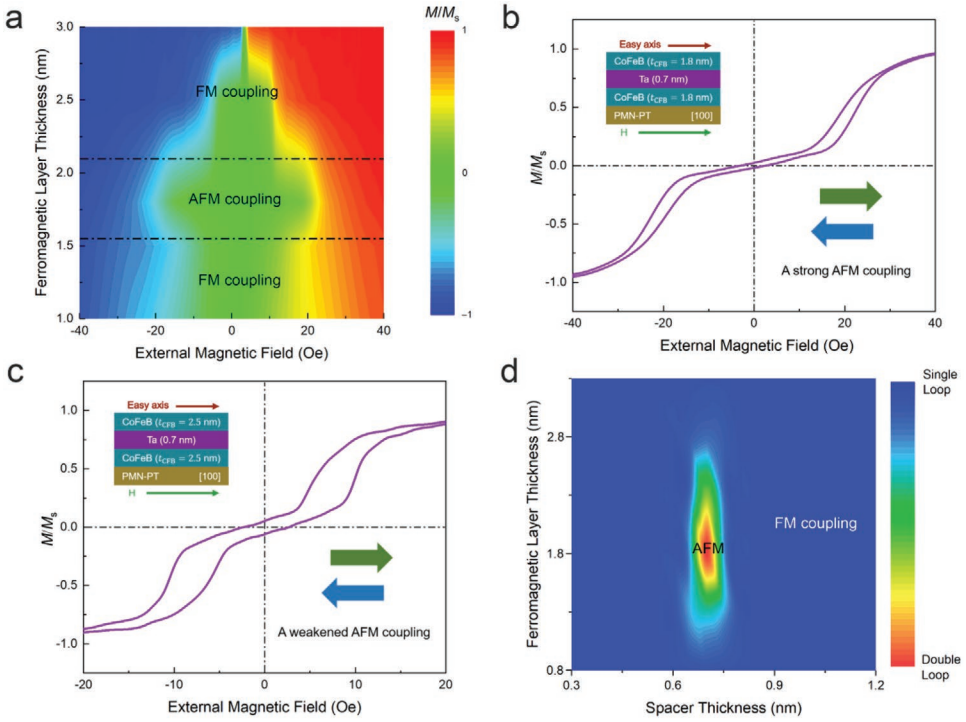

Figure 2. a) Contour plots of the easy-axis loop recorded by the sweeping static magnetic field (increasing from − 40 to + 40 Oe along the [100] direction of PMN-PT) indicate FM layer thickness dependence of IEC. b,c) Magnetic hysteresis loops at b) t_{CFB} = 1.8 nm and c) t_{CFB} = 2.5 nm, respectively. d) The corresponding RKKY interaction phase diagram summarizes the variation of hysteresis loops with FM and NM layer thicknesses.

demonstrate that the CFB/Ta/CFB heterostructure with FM coupling can be insensitive to the interlayer thickness, which benefits practical manufacturing.

So far, little attention has been paid to the effect of FM layer thickness on IEC. It is explored as shown in the contour plots (**Figure 2**a) of the easy-axis loop recorded by sweeping static *H*-field along the [100] direction in sandwich heterostructures, where the thickness of Ta is 0.7 nm. In the in-plane system, the t_{CFB} = 1.8 nm sample carries typical AFM coupling. And the magnetic reversal shows a spin-flop transition behavior.[31] It is known that the spins in the SAF structure can be divided into two main categories: surface spin (the upper FM layer) and bulk spin (the lower FM layer).[7,32] The surface spins are easier to handle than the bulk spins,[32] leading to two transition stages, as shown in Figure 2b. When t_{CFB} deviates from 1.8 nm, the AFM coupling strength is weakened, as demonstrated in Figure 2c and Figure S2 in the Supporting Information. If t_{CFB} keeps increasing or decreasing, the hysteresis loop transforms to a single-loop. The FM layer thickness effect could result from multiple reflections of electrons in the FM layers, similar to a Fabry–Pérot cavity for optical waves.[21] Figure 2d is a summary of the hysteresis loops as a function of t_{CFB} and t_{Ta}, which is a result of both the experimental data and the simulation of AFM-FM coupling status. Specifically, the blue region represents single-loop mode with two CFB moments ferromagnetically coupled. The red region shows the double-loop mode with these spins in FM layers antiparallel to each other. Similarly, this SAF structure with two FM spins parallel aligned exhibits the robustness of IEC to FM layer thickness.

The *E*-field controllable RKKY interaction is investigated by in situ VSM measurements, where a static *H*-field is applied along [100] direction. A schematic of the VSM measurement configuration is displayed in **Figure 3**a. The external *E*-field is applied to PMN-PT along [011] direction using the SAF structure as the top electrode and a sputtered Pt film as the bottom electrode. As shown in Figure 3b–d, we demonstrate the *E*-field could modify RKKY interaction at room temperature via strain. We deposit CFB 1.8 nm to study the *E*-field modification of IEC. For t_{Ta} = 0.65 nm SAF sample, the IEC is so strong that the change is small. Along the [100] direction of t_{Ta} = 0.7 nm SAF heterostructure, the hysteresis loop varies from the initial double-loop to single-loop under a 10 kV cm^{-1} *E*-field, from AFM coupling to FM coupling state. In contrast, the electrical transformation from the single-loop into a double-loop pattern can be achieved with t_{Ta} = 0.75 nm. Therefore, the external *E*-field switches the IEC modes stably and nonvolatilely. The distortion of the Fermi surface can understand the mechanism.[7,27] In detail, *E*-field-induced non-180° ferroelastic domain switching leads to the lattice reconstruction due to the electrostriction effect in the piezoelectric substrate.[29] Then, the symmetry breakup caused by the strain gives rise to the change of Fermi level.[26]

The magnetic anisotropy variations of the voltage control process are quantitatively determined by dynamic spin measurement via in situ FMR experiments in a sample where t_{CFB} = 1.8 nm and t_{Ta} = 0.7 nm when *E*-field is 0 and 10 kV cm^{-1}, respectively, as summarized in **Figure 4**a,b (typical *E*-field modulation of FMR absorption spectra along [100] and [01$\bar{1}$] can be seen in Figure S3 in the Supporting Information). The

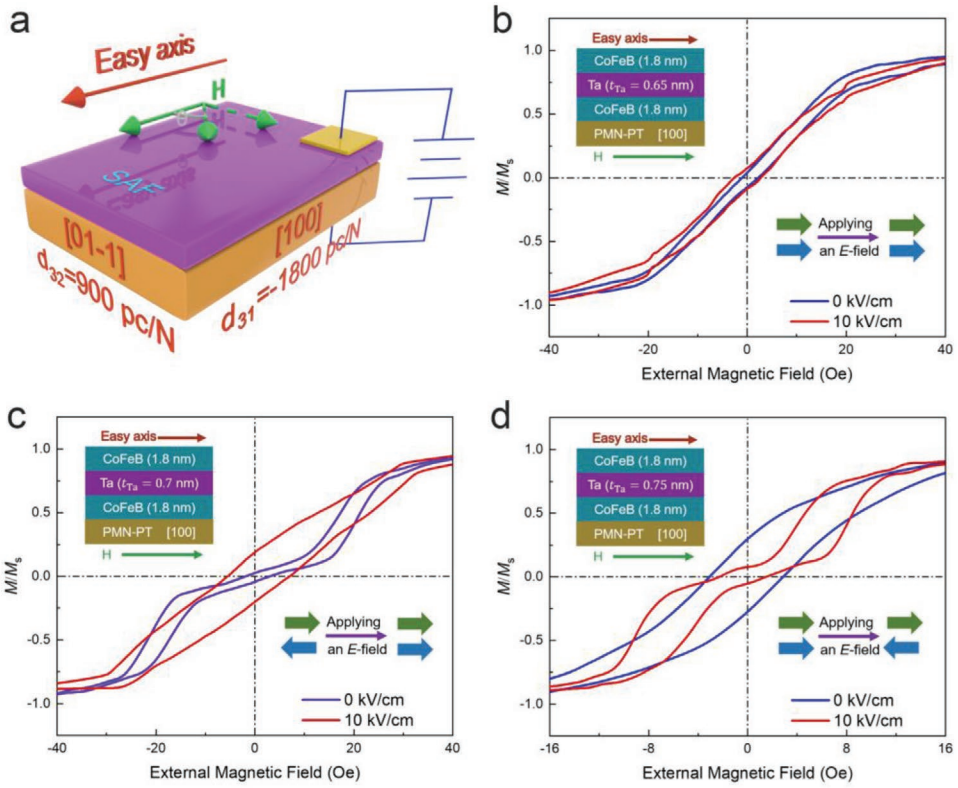

Figure 3. *E*-field control of RKKY interaction along easy-axis (the [100] direction of PMN-PT). a) Schematic of the SAF sandwich heterostructure and measurement configuration. b–d) Magnetic hysteresis loop evolution during in situ voltage regulation process in SAF sample, where t_{CFB} = 1.8 nm and b) t_{Ta} = 0.65 nm, c) t_{Ta} = 0.7 nm, and d) t_{Ta} = 0.75 nm, respectively.

magnetic field direction is rotating within the [100] direction (defined as 0°) and [$01\bar{1}$] direction of PMN-PT (defined as 90°). The dual-mode FMR spectra can be found in the SAF heterostructures with RKKY interaction and named acoustic mode (AM) and optical mode (OM).[33] The dispersion relation of AM is the same as that of a single layer because the IEC produce no dynamic contribution to the AM resonance which is due to the tight phase lock of the RF components of two magnetization vectors.[33] AM can be described as

$$\frac{f}{\gamma} = \sqrt{\left(H_{r,AM} - H_k\right)\left(H_{r,AM} + 4\pi M_s\right)} \quad (1)$$

An extra field J_{RKKY} can be introduced into the dispersion relation of the OM[34]

$$\frac{f}{\gamma} = \sqrt{\left(H_{r,OM} - H_k - J_{RKKY}\right)\left(H_{r,OM} - J_{RKKY} + 4\pi M_s\right)} \quad (2)$$

Equations (1) and (2) can give a straight forward relationship

$$J_{RKKY} = H_{r,OM} - H_{r,AM} \quad (3)$$

where f is the angular resonance frequency, γ is the gyromagnetic ratio, $H_{r,AM}$ is the AM resonance field, $H_{r,OM}$ is the OM resonance field, H_k is related to the magnetocrystalline volume anisotropy, M_s is the saturation magnetization, and J_{RKKY} is the effective RKKY interaction field.[35] According to the RKKY theory, an AFM coupling has a positive J_{RKKY} while an FM coupling has a negative value.[36] As shown in Figure 4a,b, OM mode is higher than AM mode, indicating AFM coupling. And after applying E = 10 kV cm^{-1} to PMN-PT, the AM and OM modes are closer (calculated J_{RKKY} is summarized in Figure S4 in the Supporting Information), corresponding to the trend of the change from AFM coupling to FM coupling. It is worth pointing out that AM and OM modes reverse incompletely because the FMR technology is a perturbative method.[37] Only a small number of spins during the measurement process involve.[38]

Figure 4c is a summary of the variation of easy-axis hysteresis loops under E = 0, 5, 10 kV cm^{-1}, respectively, with a static H-field along the [100] direction in a SAF heterostructure where t_{Ta} = 0.7 nm and t_{CFB} = 1.8 nm. The increasing external voltage makes the loop gradually changes from an initial double-loop to a single-loop pattern. From the perspective of the application, an *E*-field controllable RKKY switching method in a reversible and nonvolatile manner has practical application potential. As shown in Figure 3c, the relative magnetization angle in the two CFB layers is large under an external magnetic field of 1.5 Oe along [100] direction. Then two distinct remnant states of M between ≈0.11 and 0.42 M_s repeat *E*-field impulse switching of +10 and –10 kV cm^{-1} is obtained, as shown in Figure 4d. The magnetic hysteresis loops switching after 10k cycles and the electrical measurements on the SAF heterostructures are shown in Figures S5 and S7 (Supporting Information), respectively, which is of great practical value for next-generation spintronic devices, especially the emerging

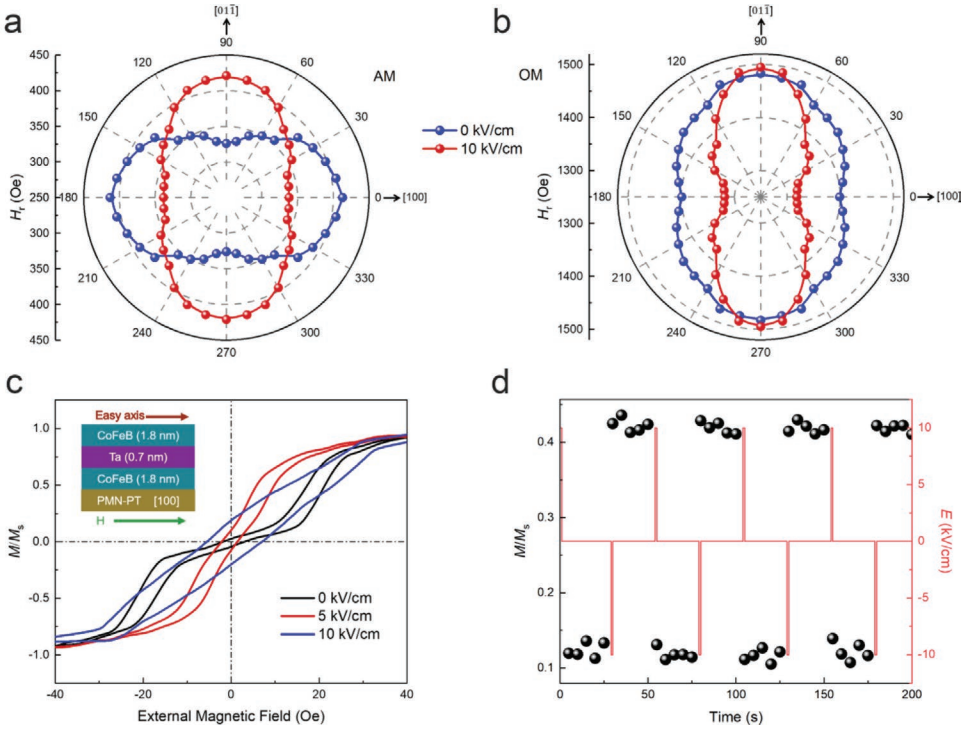

Figure 4. a,b) Angular dependence of *E*-field-induced FMR field shifts for the AFM-coupled SAF heterostructure, where $t_{Ta} = 0.7$ nm and $t_{CFB} = 1.8$ nm, along [100] direction under 0 and 10 kV cm^{-1}. The magnetic field is rotating from the [100] direction (0°) to [01$\bar{1}$] direction (90°). c) *E*-field dependence of the easy-axis hysteresis loops for the sample, where $t_{Ta} = 0.7$ nm and $t_{CFB} = 1.8$ nm along [100] direction. d) *E*-field-impulse-induced nonvolatile and reversible magnetic moment switching along [100] direction with an assisted *H*-field.

computing paradigms such as neuromorphic computing and computation-inmemory.[1,39]

3. Conclusion

In summary, no periodical oscillation with the FM layer thickness (t_{CFB}) or NM layer thickness (t_{Ta}) changing has been confirmed experimentally, and the reversible and nonvolatile modulation of the RKKY exchange coupling based on the CoFeB/Ta/CoFeB/(011)PMN-PT structures has been demonstrated, respectively. First, FM and NM layer thickness dependence of indirect interaction is confirmed via VSM. And the experiment shows no periodical oscillation, indicating the high robustness of IEC to layer thickness. Besides, single-loop and double-loop patterns are achieved, corresponding to the different extent of FM or AFM coupling. Second, we have realized *E*-field controllable transformation from single-shape to double-loop, demonstrated by VSM and FMR measurements. A stable switching of AFM and FM modes by repeated *E*-field impulse with in-plane *H*-field assistance has been proved from the device perspective. This work is a significant improvement for further understanding RKKY interaction and realizing the next generation of switchable AFM spintronics applications.

4. Experimental Section

Sample Growth: Ta (5 nm)/$Co_{40}Fe_{40}B_{20}$ (*t* nm)/Ta (*x* nm)/$Co_{40}Fe_{40}B_{20}$ (*t* nm)/Ta (5 nm) heterostructures were deposited onto (011) PMN-PT substrates by DC magnetron sputtering at room temperature. The top and bottom Ta were deposited as capping layer and seed layer, respectively. Plasma etching was used to clean the surface. The background pressure was 2×10^{-7} Torr.

Magnetic Property Measurements: The in situ VSM and FMR measurements were carried out based on a LakeShore 7404 VSM system and a JEOL FA200 electron paramagnetic resonance system, respectively. The microwave field frequency was 9.2 GHz, and the microwave power was 1 mW. The voltage was applied onto the PMN-PT substrate along [011] direction by Keithley 6517b electrometer, using the SAF structure as the top electrode and a Pt film deposited on the backside of PMN-PT as the bottom electrode. All measurements were conducted at room temperature.

Supporting Information

Supporting Information is available from the Wiley Online Library or from the author.

Acknowledgements

This work was supported by the National Natural Science Foundation of China (Nos. 52175434, 52172126, 62001366, 91964109, 11804266, and 11534015), the National Key R&D Program of China (2018YFB0407601, 2019YFA0307900), and the Fundamental Research Funds for the Central Universities (xjh012019042), and the National 111 Project of China (B14040), and the China Postdoctoral Science Foundation (No. 2021T140549).

Conflict of Interest

The authors declare no conflict of interest.

Data Availability Statement

The data that support the findings of this study are available from the corresponding author upon reasonable request.

Keywords

antiferromagnetic spintronics, *E*-field control, interlayer exchange coupling, magnetoelectric coupling, RKKY

Received: January 2, 2022
Revised: March 13, 2022
Published online: April 3, 2022

[1] K. Roy, A. Jaiswal, P. Panda, *Nature* **2019**, *575*, 607.
[2] M. Romera, P. Talatchian, S. Tsunegi, F. A. Araujo, V. Cros, P. Bortolotti, J. Trastoy, K. Yakushiji, A. Fukushima, H. Kubota, S. Yuasa, M. Ernoult, D. Vodenicarevic, T. Hirtzlin, N. Locatelli, D. Querlioz, J. Grollier, *Nature* **2018**, *563*, 230.
[3] J. Torrejon, M. Riou, F. A. Araujo, S. Tsunegi, G. Khalsa, D. Querlioz, P. Bortolotti, V. Cros, K. Yakushiji, A. Fukushima, H. Kubota, S. Y. Uasa, M. D. Stiles, J. Grollier, *Nature* **2017**, *547*, 428.
[4] K. M. Krasikov, A. V. Bogach, S. V. Demishev, V. V. Voronov, N. Y. Shitsevalova, V. B. Filipov, N. E. Sluchanko, *J. Magn. Magn. Mater.* **2022**, *545*, 168796.
[5] T. Jungwirth, X. Marti, P. Wadley, J. Wunderlich, *Nat. Nanotechnol.* **2016**, *11*, 231.
[6] J. Zelezny, H. Gao, K. Vyborny, J. Zemen, J. Masek, A. Manchon, J. Wunderlich, J. Sinova, T. Jungwirth, *Phys. Rev. Lett.* **2014**, *113*, 157201.
[7] Q. Yang, L. Wang, Z. Y. Zhou, L. Q. Wang, Y. J. Zhang, S. S. Zhao, G. H. Dong, Y. X. Cheng, T. Min, Z. Q. Hu, W. Chen, K. Xia, M. Liu, *Nat. Commun.* **2018**, *9*, 991.
[8] R. A. Duine, K. J. Lee, S. S. P. Parkin, M. D. Stiles, *Nat. Phys.* **2018**, *14*, 217.
[9] R. Y. Chen, Q. R. Cui, L. Y. Liao, Y. M. Zhu, R. Q. Zhang, H. Bai, Y. J. Zhou, G. Z. Xing, F. Pan, H. X. Yang, C. Song, *Nat. Commun.* **2021**, *12*, 3113.
[10] T. Jungwirth, J. Sinova, A. Manchon, X. Marti, J. Wunderlich, C. Felser, *Nat. Phys.* **2018**, *14*, 200.
[11] B. Dieny, I. L. Prejbeanu, K. Garello, P. Gambardella, P. Freitas, R. Lehndorff, W. Raberg, U. Ebels, S. O. Demokritov, J. Akerman, A. Deac, P. Pirro, C. Adelmann, A. Anane, A. V. Chumak, A. Hirohata, S. Mangin, S. O. Valenzuela, M. C. Onbasli, M. D'Aquino, G. Prenat, G. Finocchio, L. Lopez-Diaz, R. Chantrell, O. Chubykalo-Fesenko, P. Bortolotti, *Nat. Electron.* **2020**, *3*, 446.
[12] L. Q. Liu, C. F. Pai, Y. Li, H. W. Tseng, D. C. Ralph, R. A. Buhrman, *Science* **2012**, *336*, 555.
[13] L. Q. Liu, O. J. Lee, T. J. Gudmundsen, D. C. Ralph, R. A. Buhrman, *Phys. Rev. Lett.* **2012**, *109*, 096602.
[14] I. M. Miron, G. Gaudin, S. Auffret, B. Rodmacq, A. Schuhl, S. Pizzini, J. Vogel, P. Gambardella, *Nat. Mater.* **2010**, *9*, 230.
[15] A. Brataas, A. D. Kent, H. Ohno, *Nat. Mater.* **2012**, *11*, 372.
[16] Y. Niimi, Y. Kawanishi, D. H. Wei, C. Deranlot, H. X. Yang, M. Chshiev, T. Valet, A. Fert, Y. Otani, *Phys. Rev. Lett.* **2012**, *109*, 156602.
[17] S. Woo, M. Mann, A. J. Tan, L. Caretta, G. S. D. Beach, *Appl. Phys. Lett.* **2014**, *105*, 212404.
[18] H. Sato, M. Yamanouchi, S. Ikeda, S. Fukami, F. Matsukura, H. Ohno, *Appl. Phys. Lett.* **2012**, *101*, 022414.
[19] S. S. P. Parkin, *Phys. Rev. Lett.* **1991**, *67*, 3598.
[20] S. N. Okuno, K. Inomata, *Phys. Rev. Lett.* **1994**, *72*, 1553.
[21] P. Bruno, *Europhys. Lett.* **1993**, *23*, 615.
[22] P. Bruno, *J. Magn. Magn. Mater.* **1993**, *121*, 248.
[23] P. Bruno, C. Chappert, *Phys. Rev. Lett.* **1991**, *67*, 1602.
[24] M. T. Johnson, R. Coehoorn, J. J. Devries, N. W. E. Mcgee, J. A. Destegge, P. J. H. Bloemen, *Phys. Rev. Lett.* **1992**, *69*, 969.
[25] E. E. Fullerton, M. J. Conover, J. E. Mattson, C. H. Sowers, S. D. Bader, *Phys. Rev. B* **1993**, *48*, 15755.
[26] X. J. Wang, Q. Yang, L. Wang, Z. Y. Zhou, T. Min, M. Liu, N. X. Sun, *Adv. Mater.* **2018**, *30*, 1803612.
[27] Q. Yang, Z. Y. Zhou, L. Q. Wang, H. J. Zhang, Y. X. Cheng, Z. Q. Hu, B. Peng, M. Liu, *Adv. Mater.* **2018**, *30*, 1800449.
[28] W. Zhao, J. Kim, X. X. Huang, L. Zhang, D. Pesquera, G. A. P. Velarde, T. Gosavi, C. C. Lin, D. E. Nikonov, H. Li, I. A. Young, R. Ramesh, L. W. Martin, *Adv. Funct. Mater.* **2021**, *31*, 2105068.
[29] B. Peng, Z. Y. Zhou, T. X. Nan, G. H. Dong, M. M. Feng, Q. Yang, X. J. Wang, S. S. Zhao, D. Xian, Z.-D. Jiang, W. Ren, Z. G. Ye, N. X. Sung, M. Liu, *ACS Nano* **2017**, *11*, 4337.
[30] Y. J. Li, C. L. Li, Q. Lu, Q. Du, K. Q. Shi, Z. Q. Hu, Z. Y. Zhou, M. Liu, J. Y. Pan, *J. Phys. Chem. C* **2021**, *125*, 24025.
[31] A. N. Bogdanov, A. V. Zhuravlev, U. K. Rossler, *Phys. Rev. B* **2007**, *75*, 094425.
[32] S. G. E. te Velthuis, J. S. Jiang, S. D. Bader, G. P. Felcher, *Phys. Rev. Lett.* **2002**, *89*, 127203.
[33] S. D. Li, Q. Li, J. Xu, S. S. Yan, G. X. Miao, S. S. Kang, Y. Y. Dai, J. Q. Jiao, Y. G. Lu, *Adv. Funct. Mater.* **2016**, *26*, 3738.
[34] B. Heinrich, J. F. Cochran, M. Kowalewski, J. Kirschner, Z. Celinski, A. S. Arrott, K. Myrtle, *Phys. Rev. B* **1991**, *44*, 9348.
[35] X. Xing, M. Liu, S. D. Li, O. Obi, J. Lou, Z. Zhou, B. Chen, N. X. Sun, *IEEE Trans. Magn.* **2011**, *47*, 3104.
[36] Y. Gong, Z. Cevher, M. Ebrahim, J. Lou, C. Pettiford, N. X. Sun, Y. H. Ren, *J. Appl. Phys.* **2009**, *106*, 063916.
[37] H. W. Xi, R. M. White, S. M. Rezende, *Phys. Rev. B* **1999**, *60*, 14837.
[38] V. I. Nikitenko, V. S. Gornakov, L. M. Dedukh, Y. P. Kabanov, A. F. Khapikov, A. J. Shapiro, R. D. Shull, A. Chaiken, R. P. Michel, *Phys. Rev. B* **1998**, *57*, R8111.
[39] X. Mou, J. S. Tang, Y. J. Lyu, Q. T. Zhang, S. Y. Yang, F. Xu, W. Liu, M. H. Xu, Y. Zhou, W. Sun, Y. A. Zhong, B. Gao, P. Yu, H. Qian, H. Q. Wu, *Sci. Adv.* **2021**, *7*, eabh0648.

